Physica Scripta

PAPER

Structural and optical parameters of polyvinyl alcohol films reinforced with Mn_2O_3/reduced graphene oxide composite

T S Soliman[1,2,*], **S A Vshivkov**[2], **Ahmed I Abdel-Salam**[3], **Islam Gomaa**[3] and **A Khalid**[4]

[1] Physics Department, Faculty of Science, Benha University, Benha 13518, Egypt
[2] Institute of Natural Sciences and Mathematics, Ural Federal University, Ekaterinburg 620000, Russia
[3] Nanotechnology Research Centre (NTRC), The British University in Egypt (BUE), El-Shorouk City, Suez Desert Road, PO Box 43, Cairo 11837, Egypt
[4] Department of Basic Engineering Sciences, Faculty of Engineering (Shoubra), Benha University, Benha, Egypt
[*] Author to whom any correspondence should be addressed.

E-mail: tarek.attia@fsc.bu.edu.eg

Keywords: polymer composites, UV-visible spectroscopy, refractive index, Mn_2O_3/rGO

RECEIVED
23 October 2022

REVISED
5 December 2022

ACCEPTED FOR PUBLICATION
14 December 2022

PUBLISHED
23 December 2022

Abstract

The novel polyvinyl alcohol (PVA) films reinforced with varied concentrations of Mn_2O_3/reduced graphene oxide (rGO) nanoparticles (NP) are prepared via the casting technique. A hydrothermal approach methodology is used to prepare manganese oxide reduce graphene oxide (Mn_2O_3/rGO) composite. The X-ray diffraction (XRD), Fourier transform infrared (FTIR), scanning electron microscope (SEM), and optical microscope setups are used to study the impact of nanoparticles on the structure of the PVA matrix. The surface roughness was measured and found to increase with increasing NPs concentration in the polymer matrix. The UV–vis spectroscopy is used to investigate the optical absorption and transmission data for the prepared films. The addition of Mn_2O_3/rGO NP in the polymer matrix effects on the optical parameters like the absorption coefficient, optical bandgap, refractive index, and optical conductivity. The optical bandgap of PVA films with Mn_2O_3/rGO NP is lower than that of PVA pure. The refractive index and optical conductivity were tuned with the addition of Mn_2O_3/rGO NP. The PVA-Mn_2O_3/rGO films are promising material for various opto-electronic fields.

1. Introduction

The investigation of polymer composites containing transition metals are particularly interested in opto-electronic applications like; the sensors, communications, shielding, electronic components, photocatalyst, batteries and solar cells [1, 2]. Polyvinyl alcohol (PVA) is considered as one of the most well-known water-soluble polymers utilized in a variety of electronic applications. This is related to the excellent properties of easy forming films, high optical and dielectric properties. Recently, several nanofillers (metals, metal oxides, transition metals such as; Fe [3], Ni [4], Si [5], Al [6], SiO2 [7], ZnO [8], CuO [9], $BaTiO_3$ [10], Fe_2O_3 or NiO [11], TiO_2 [12], Erbium [13], CdSe [14], and carbon dots and nanotubes [15, 16]) have been inserted in the PVA matrices for enhancement their properties. All these studies and more have been done to improve the structure and physical properties, especially the optical and electrical properties, for use in various industrial fields.

Manganese oxide (Mn_2O_3) is one of transition metal oxides that is candidate for various applications like batteries, photocatalyst, supercapacitors, and sensors [17–20]. Mn_2O_3 has many advantage like; nontoxicity, stable, cheap, and good electrochemical performance in aqueous electrolyte medium [21]. Several methods were used to enhance the performance of the transition metal oxides including change of the particle shape, or size, or by doping with different materials. Various systems have used rGO for enhance the structural and optical parameters of the materials such as; CdSe-rGO [22, 23], SnO_2-rGO [24], a-Fe_2O_3/SnO_2/rGO [25], Fe_2O_3–rGO & MgO-rGO [26], and $NiCo_2S_4$-rGO [27]. Vignesh *et al* [21], Sharma *et al* [28], Gnanam *et al* [29], and Javed *et al* [30] have synthesized Mn_2O_3 with different techniques and studied their structure and optical parameters.

Recently, Kalaiselvi *et al* [31] have studied the impact of different graphene oxide concentrations on the structure and optical properties of Mn_2O_3. An enhancement in the properties was observed due to the presence of the graphene oxide in the matrix.

The investigations of PVA doped with Mn_2O_3 NP composite are very rare in the literature. The effect of Mn_2O_3 on the structure and optical properties of PVA have been investigated previously. Khairy *et al* [32] synthesized Mn_2O_3 nanoparticles using the combustion method, inserted these nanoparticles in the PVA matrix, and found a change in the structure of PVA films and the enhancement of their optical parameters. Aslam *et al* [33] have studied the impact of graphene oxide (GO) sheets on the structural and optical properties of PVA films, where improvements in the film absorption was observed because of the increasing in the hydrogen bonds between the PVA matrix and GO sheets.

Recently, Badawi and Alharthi [34] have fabricated PVA films blended with rGO sheets and studied the effect of different metal oxides (Fe_2O_3, Pb_3O_4, and MnO_2) on their physical properties. They found an enhancement in the optical, electrical, and mechanical properties with the incorporation of the metal oxides to the PVA-rGO blend system. For our knowledge, the information about the study of rGO impact on the structural and optical properties of Mn_2O_3 is very rare and as well for the PVA- Mn_2O_3/rGO films are absent. So, the motivation of this work is to enhance and tune the optical parameters of the polymer films with the nanoparticles of Mn_2O_3 decorated on the rGO sheets which has not been discussed previously.

Herein the Mn_2O_3 nanoparticles were synthesized and then decorated on the rGO sheets. The prepared Mn_2O_3/rGO nanocomposites were inserted with different concentrations in the PVA matrix and the structural and optical properties were investigated. The structure and optical characteristics of PVA-Mn_2O_3/rGO films were investigated via XRD, FTIR, optical microscope, and UV-visible spectroscopy.

2. Materials and methods

2.1. Synthesis of Mn_2O_3/rGO

The Mn_2O_3 nanoparticles have been synthesized via the hydrothermal method [27]. A solution of 20 mmole Ascorbic acid anhydrous/50 ml deionized water (DIW) was added dropwise to a solution of 30 mmole Manganese (II) acetate tetrahydrate/50 ml DIW under stirring for 15 min. This mixture was loaded into Teflon-lined autoclave and heated at the temperature of 180 °C for 2 h. The precipitation was collected by centrifugation at 8000 rpm and cooled to room temperature. The product was washed several times with deionized water, dried at 80 °C for 24 h, and then calcined at 550 °C for 2 h. This chemical process can be described according to the following chemical equation:

$$Mn(Ascrobate)_2.H_2O \xrightarrow{550\ ^\circ C} Mn_2O_3 + CO_2 + H_2O$$

Finally, the Mn_2O_3 and GO were mixed in 100 ml DIW and sonicated for 15 min. The GO was reduced to form rGO through the sonication process [35, 36].

2.2. Preparation of PVA-Mn_2O_3/rGO films

The polyvinyl alcohol (PVA, $M_w = 1 \times 10^6$) solution was prepared by dissolving 4 gm PVA powder in 80 ml of DIW at 70 °C. This mix was stirred for several hours until obtaining clear solution. After that the solution was divided in four boxes to obtain four samples: one of them is the pure PVA solution and the other three sample were used for preparing of mixes with different concentrations of Mn_2O_3/rGO NP. The Mn_2O_3/rGO NP were dispersed in the PVA solution via sonication process (Ultrasonic processor, CPX-750 Cole-Parmer). The sonication process was continued for 5 min at room temperature, and then the mix was casted in polypropylene dishes and left for drying at 25 °C in dry atmosphere for a week. The concentrations of Mn_2O_3/rGO NP loaded in the solutions were 0.5, 1.0, and 1.5 wt.% which labeled as M1, M2, and M3, respectively. The produced films had a thickness of around 100 μm, were measured by a micrometer. Figure 1 shows the color gradient of pure PVA and PVA-Mn_2O_3/rGO films.

2.3. Characterization and setups

The XRD and optical microscope were used to investigate the effect of Mn_2O_3/rGO NP on the structure of the PVA films. XRD analysis was done via Bruker D8 diffractometer (with Cu-Kα radiation, $\lambda = 1.5418$ Å). Fourier transform infrared (FTIR) was used to identify the chemical bonds formed in the polymer matrix and show the effect of doping on these bonds. FTIR spectrometer (model Vertex 70-Bruker, Germany) was used under the wavenumber range from 4000 to 400 cm^{-1} with 4 cm^{-1} resolution. The Mn_2O_3/rGO NP morphology in the PVA matrix was investigated via the optical microscope OLYMPUS-BX51 and scanning electron microscope (SEM, Merlin, Carl-Zeiss LEO982). The analysis of the surface roughness parameters was measured using Surface Roughness Tester SRT-6600. The measurement mechanism depends on the sensor contacts method.

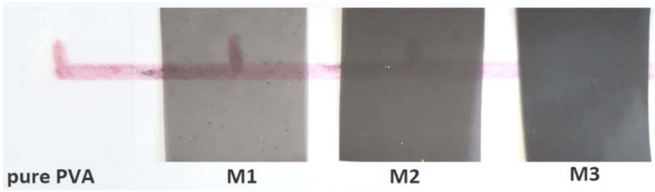

Figure 1. The color gradient of pure PVA and PVA-Mn_2O_3/rGO samples.

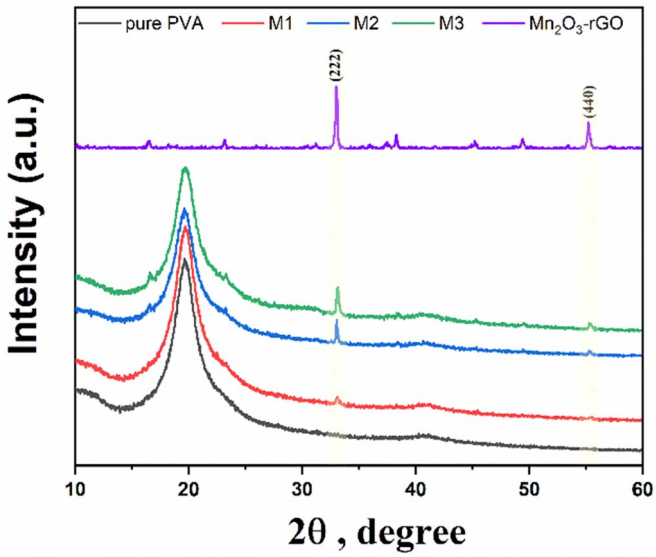

Figure 2. XRD patterns for PVA-Mn_2O_3/rGO composite films.

The obtained measurements were repeated five times to be affirmed and more accurate. A low-temperature nitrogen vapor sorption method was used to evaluate the specific surface area and porous structure parameters of the polymers. Measurements were carried out using a TRISTAR 3020 automatic surface and porosity gas adsorption analyzer from Micromerics (USA), which implements a volumetric version of the sorption method. The TRISTAR 3020 analyzer allows to automatically obtain an adsorption and desorption isotherm with a given number of experimental points, on the basis of which to calculate the specific surface area of the sample according to the BET method, the total pore volume by the maximum adsorption value and the pore volume distribution curve by size. Before the sorption experiment, volatile components were removed from the samples by evacuation at a residual pressure of 10^{-2} atm and T = 70.0 °C to a constant weight. As a result of the experiment, it was found that the samples did not absorb nitrogen vapors, which does not allow calculating surface parameters and porosity. According to the range of values of the parameters to be determined, this means that value of specific surface area of samples $S_{sp} < 0.01$ m^2 g^{-1}, the total pore volume W_0 does not exceed the value of $4{\cdot}10^{-6}$ cm^3 g^{-1}.

The UV-Visible spectrometer (model-Cary5000) was used to investigate the absorption and transmission spectra of the prepared films.

3. Results and discussion

3.1. Structure analysis

The XRD spectra of pure PVA, Mn_2O_3/rGO composite, and PVA reinforced by Mn_2O_3/rGO nanoparticles with different contents are displayed in figure 2.

A broad hump at 19.66° related to (101) plane was observed. It reflects the semicrystalline nature of the PVA films [5]. As the concentration of Mn_2O_3/rGO NP increases the broadness of the hump increases as well. Wherein a new peak at 33.005° is observed. As the concentration of Mn_2O_3/rGO NP increases the peak intensity increases as well. This peak and the other at 55.21° are observed at higher Mn_2O_3/rGO NP concentration are

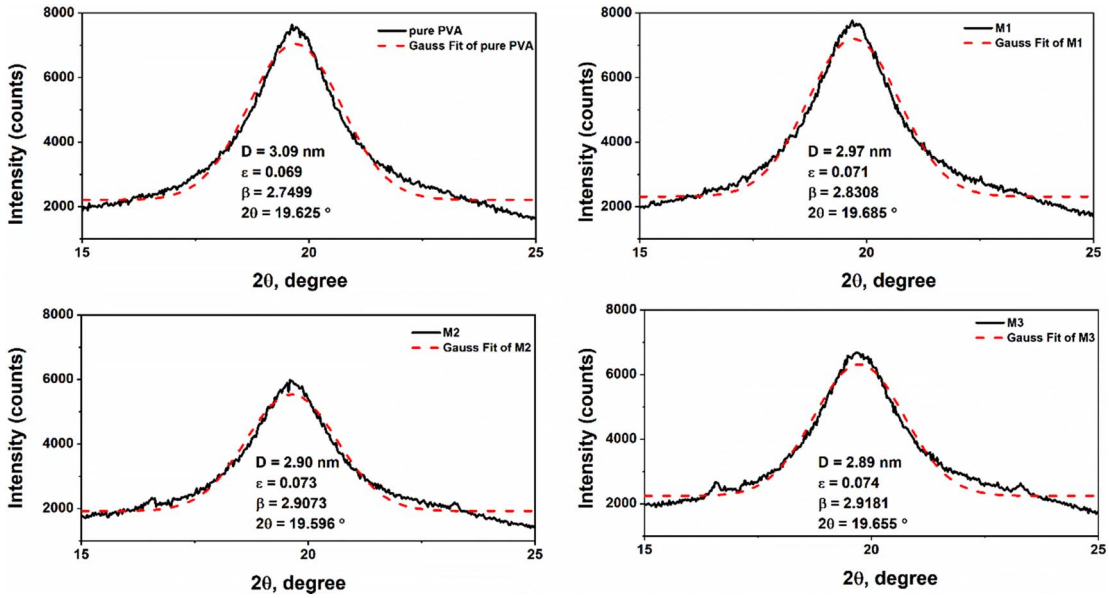

Figure 3. Gaussian fitting of (101) XRD peak for PVA-Mn_2O_3/rGO composite films.

Table 1. Geometrical parameters of PVA-Mn_2O_3/rGO composite films.

Sample	2θ (°)	FWHM (°)	D (nm)	ε	$\delta \times 10^{17}$, m^{-2}	Crystallinity degree, %
pure PVA	19.6254	2.74988	3.06	0.069	1.07	56.3
M1	19.6850	2.83084	2.97	0.071	1.13	55.3
M2	19.5956	2.90734	2.90	0.073	1.19	53.7
M3	19.6552	2.91809	2.89	0.074	1.20	52.8

related to the cubic phase of Mn_2O_3 NP (JCPDS: 41-1442). The peaks at 33.005° and 55.21° are indexed to (222) and (440) diffraction planes [30], respectively.

Additional analysis of the characteristic peak (101) was done to calculate the cluster size (D), the internal strain (ε), and dislocation density (δ) of the material using the Gaussian fitting process. This can be calculated by the following equations [37, 38],

$$D = \frac{0.9\ \lambda}{\beta \cos \theta} \tag{1}$$

$$\varepsilon = \frac{\beta}{4 \tan} \tag{2}$$

$$\delta = \frac{1}{D^2} \tag{3}$$

The full width at half-maximum (β) and the Bragg's angle (θ) were extracted from the Gaussian fitting to the (101) hump, as presented in figure 3. These data were used to calculate the cluster size with the help of the Scherrer equation (equation (1)) [39]. The obtained data are presented in table 1 and shown in figure 3.

It is obvious that the D value decreases with an increase in Mn_2O_3/rGO NP concentration in the matrix, form 3.09 nm for pure PVA to 2.89 nm for higher Mn_2O_3/rGO NP concentration. This can be related to the interaction of the Mn_2O_3/rGO NP with the −OH groups of the PVA matrix which produces hydrogen bonding between them and causes decrement in the interchain separation of the PVA matrix [5, 40]. Whilst ε and δ increase with the increase in the Mn_2O_3/rGO concentration. The crystallinity degree decreases with the addition of Mn_2O_3/rGO NP into the PVA matrix. This result can be confirmed by computing the crystallinity degree using the following equation [41];

$$Crystallinity\ degree,\ \% = \frac{A_{(101)}}{A_c} \times 100 \tag{4}$$

where $A_{(101)}$ is the area of the (101) peak and A_c is the area of the whole curve (amorphous and crystalline) The calculated values of crystallinity degree are presented in table 1. It is shown that the crystallinity degree decreased

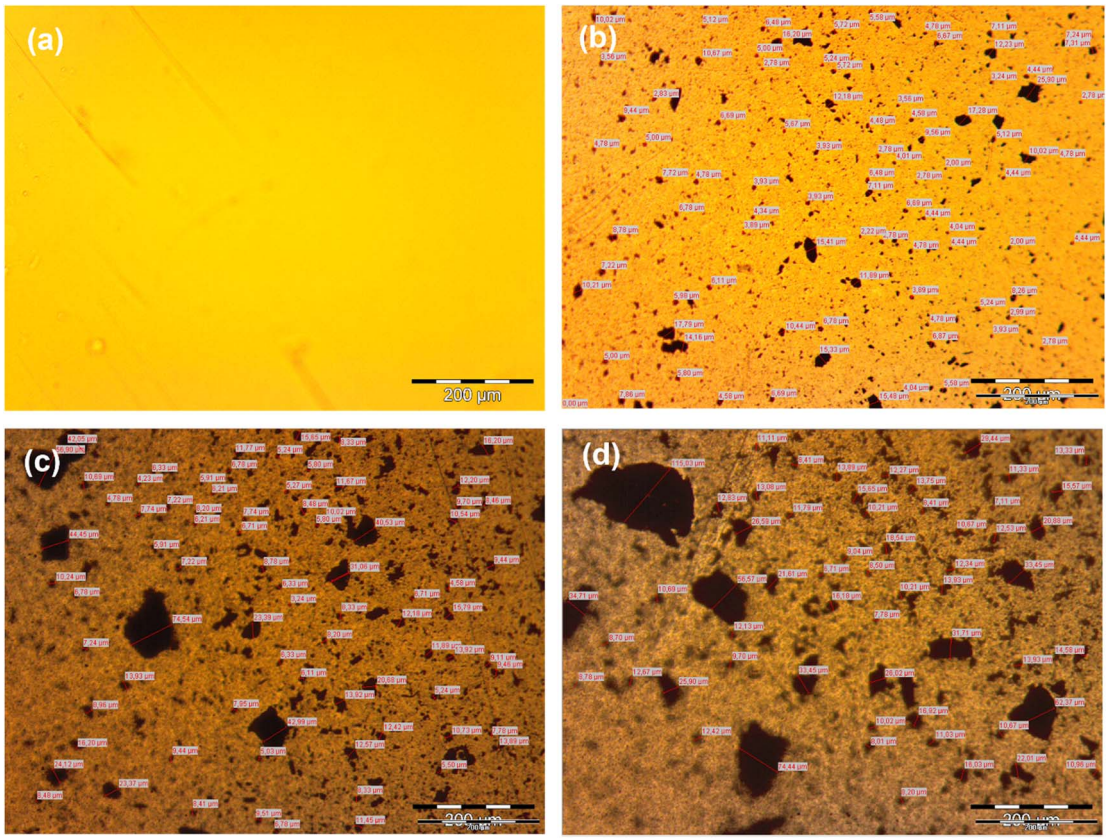

Figure 4. Optical microscope images for PVA-Mn_2O_3/rGO composite films; (a) pure PVA, (b) M1, (c) M2, and (d) M3.

from ~ 56% for pure PVA to ~ 52% for the higher Mn_2O_3/rGO NP concentration. This can be associated with the hydrogen-bonding between the Mn_2O_3/rGO NP and the OH-group of PVA [41].

Figure 4 shows the bright-field images of the PVA and PVA-Mn_2O_3/rGO composite films. Figure 4(a) shows the pure PVA film image. It shows a pure film without imperfections. Figures 4(b)–(d) shows PVA films with different Mn_2O_3/rGO concentrations. It is clear that the insertion of the Mn_2O_3/rGO NP in the PVA film shows rough surface. This can be related to the dispersion of the NP on the PVA matrix. Besides, as the Mn_2O_3/rGO concentration increases, the free Mn^{+3} ions density increases in the film as well. Moreover, it shows a high roughness at higher concentration and clusters formed with increasing the NP concentration as well. The clusters are formed due to NPs agglomeration because the Mn_2O_3 and rGO are polar particles, which can interact with each other due to dipole interactions. This obviously affects the optical absorption and transmission of the PVA films.

Also, the particle size distribution was investigated to clarify the growth of the particle size with increasing the Mn_2O_3/rGO concentration in the polymer matrix, as shown in figure 5. The minimum and maximum particle sizes for samples M1, M2, and M3 are 2, 3, and 6 μm and 24, 74, 115 μm, respectively. Obviously, the particle size increases as the Mn_2O_3/rGO concentration increases which is related to the agglomerations. This could be related to the increase in the density of the particles in the polymer matrix which causes an increase of the adhesion between particles to each other. Hence, agglomerations are formed.

Moreover, to be more in-depth in morphological study, the SEM analysis was investigated. Figure 6 shows the SEM images of PVA-Mn_2O_3/rGO films.

As shown no cracks are observed and the surface morphology changes with the addition of NPs in the polymer matrix, and the surface roughness increases as a result of particles agglomeration. Also, from figure 6(c), it is observed that the particles are grouped in clusters of about ~ 500–1000 nm. Furthermore, an interface was observed between nanoparticles and the polymer matrix which confirming the strong interaction and the H-bond formation between the NPs and the OH-groups of the PVA [3].

To confirm such inclusion, the surface roughness of the samples was measured via the surface roughness technique (SRT). The arithmetic mean height of the roughness profile (R_a), the root mean square roughness R_q, the maximum profile peak height (R_p), the maximum profile valley depth (R_v), and the maximum height of the profile ($R_z = R_p + R_v$) are surface parameters which are investigated via the SRT [42, 43]. The R_a, R_q, R_z, R_p, and R_v values are extracted from roughness curve (figure 6(d)) and summarized in table 2.

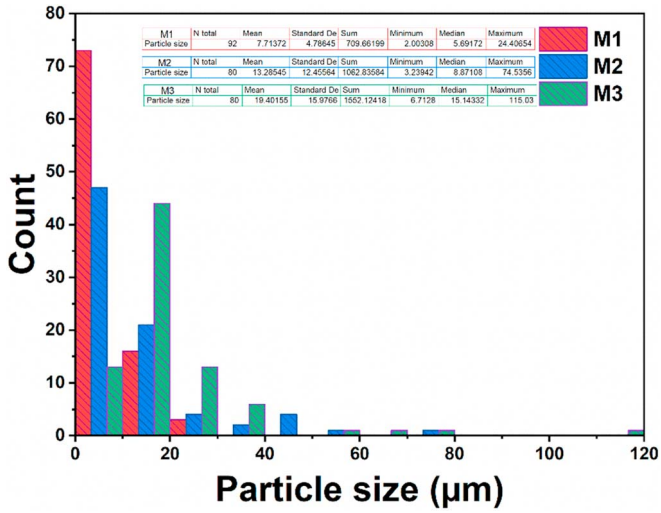

Figure 5. Histogram of the particle size distribution of the samples M1, M2, and M3 obtained from the optical microscope.

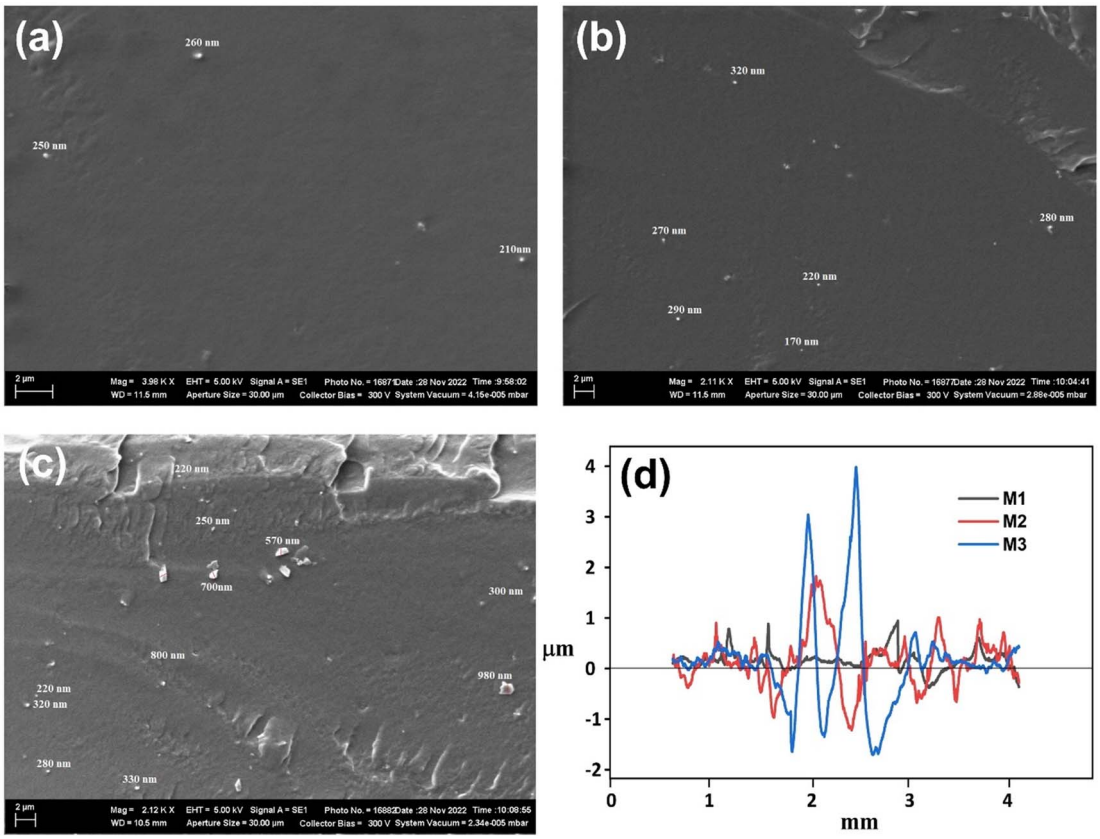

Figure 6. SEM images of; (a) M1, (b) M2, (c) M3 samples, and (d) Roughness curve.

Table 2. Surface roughness parameters of samples M1, M2, and M3.

Sample	R_a	R_q	R_z	R_p	R_v
M1	0.154	0.211	1.038	0.703	0.335
M2	0.440	0.549	2.382	1.305	1.077
M3	0.642	0.833	3.182	1.868	1.315

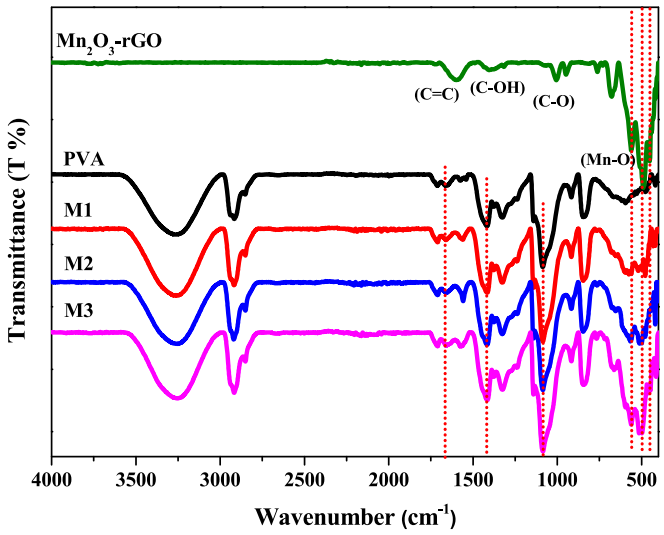

Figure 7. FTIR spectra of Mn_2O_3-rGO nanocomposite, pure PVA, and PVA- Mn_2O_3/rGO films.

As shown the Ra, R_q, R_z, R_p, and R_v values increase with the increase in Mn_2O_3/rGO NPs in the polymer matrix. This could be related to the increase of the particle sizes due to agglomerations, and this is the main reason for the increase of the surface roughness of the polymer films which is in a good accordance with the literature [44, 45].

3.2. FTIR analysis

Figure 7 shows the FTIR spectra of the Mn_2O_3-rGO nanocomposite, pure PVA, and PVA-Mn_2O_3/rGO films with different Mn_2O_3-rGO concentrations.

The FT-IR spectra of the Mn_2O_3-rGO nanocomposite revealed distinct peaks at about 554 cm^{-1}, 490 cm^{-1}, and 450 cm^{-1} are assigned to the stretching vibration of Mn–O bond of the Mn_2O_3 nanoparticles [31]. Furthermore, the peaks appeared at 1600 cm^{-1}, 1386 cm^{-1}, and 1012 cm^{-1} are characteristic for the C=C, C–OH, and C–O of the rGO, respectively [46, 47]. The FT-IR spectra of the PVA-Mn_2O_3/rGO films reveal the characteristic peaks of the Mn_2O_3-rGO, confirming presence of the Mn_2O_3-rGO after forming the polymer films. PVA reveals three characteristic peaks are observed at 3274 cm^{-1}, 1425 cm^{-1}, and 1088 cm^{-1} which are attributed to hydroxyl (O–H) group, C–OH stretching vibration, and stretching band of C–O group, respectively [33, 48]. The C–OH and C–O bonds of the GO disappeared indicating the intermolecular hydrogen bonding with the −OH groups of the PVA [33]. Furthermore, as the Mn_2O_3-rGO concentration increases in the polymer matrix, the band intensity observed for the Mn–O bonds increases and become more pronounced. This confirms the formation of hydrogen bonding and crosslinking between the polymer molecules and the nanoparticles [32, 34]. Consequently, a modification in the optical properties of the polymer films is expected.

3.3. UV-visible data

Figure 8(a) shows the UV–visible absorption spectra of PVA-Mn_2O_3/rGO composite films. The absorption edge was observed in the UV-region and shifted significantly toward the visible region with increasing the Mn_2O_3/rGO concentration in the matrix. It may be caused by the growth of the filler size and/or by the increase in the Mn^{+3} free ions in the PVA matrix with the increase in the Mn_2O_3/rGO concentration [21]. In addition, the more hydrogen bonds formed between the rGO sheets and the PVA molecules as proved in the FTIR analysis, which causes increment in the polymer films absorption as well [33]. Furthermore, the observed bands at 280 nm and 340 nm for the pure PVA are related to the (π–π^*) and (n –π^*) transitions, respectively [49, 50]. With the addition of the NP in the matrix, two wide bands are observed in the visible region at 410 and 570 nm. These bands become more pronounced at higher Mn_2O_3/rGO NP concentration. These bands are caused by the surface plasmon resonance (SPR) due to the existence of trivalent manganese ions (Mn^{3+}) in Mn_2O_3 [50]. As the PVA- Mn_2O_3/rGO film is exposed to electromagnetic waves, a SPR absorption formed from the free Mn^{3+} ions [51, 52].

Figure 8(b) illustrates the transmission spectra of PVA-Mn_2O_3/rGO composite films. As the Mn_2O_3/rGO concentration in the PVA matrix increases, the transmission of the films decreases. This can be caused by the increase in the Mn^{+3} free ion numbers which absorb more energy and the film transmittance decreases [21]. The pure PVA film transmission was about 90% which decreases gradually to about 1% at higher concentration of

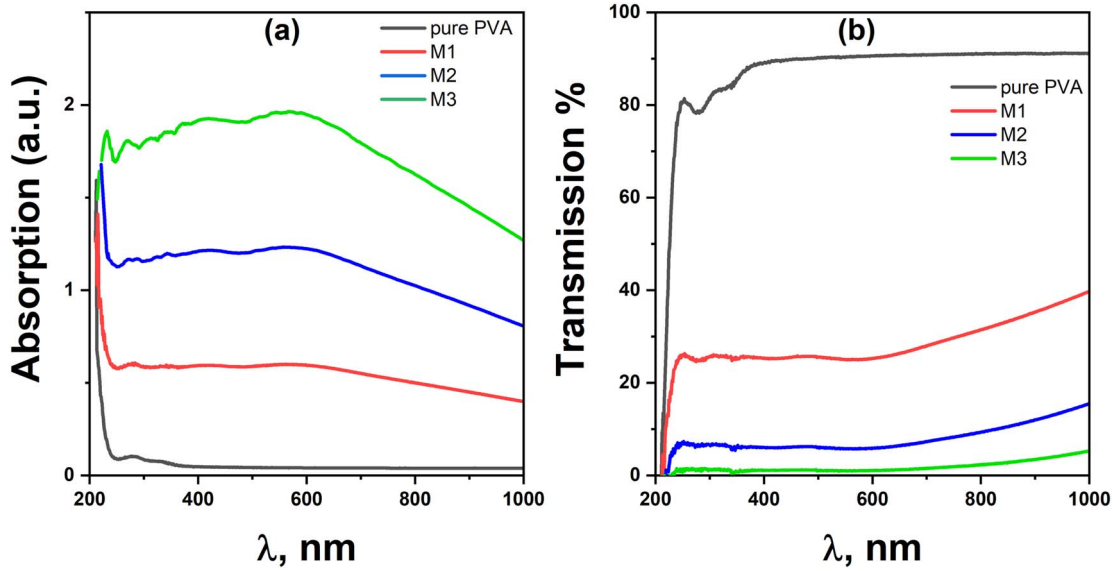

Figure 8. UV-visible spectra for PVA-Mn_2O_3/rGO composite films.

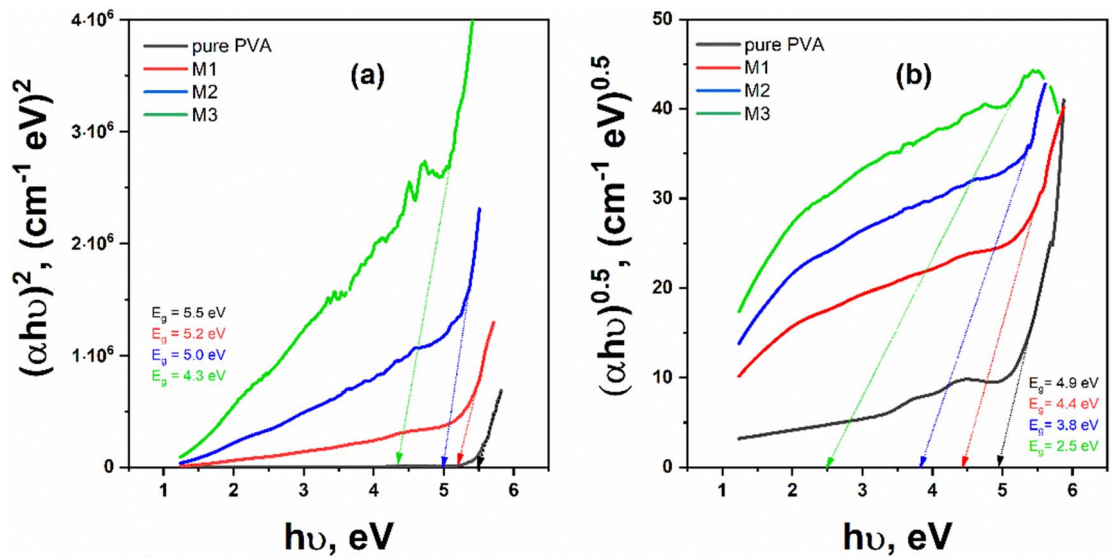

Figure 9. Plot of (a) $(\alpha h\upsilon)^2$ and (b) $(\alpha h\upsilon)^{0.5}$ versus $h\upsilon$ for PVA-Mn_2O_3/rGO composite films.

the nanoparticles. Such material with lower transmission makes the obtained polymer films promising candidate in UV protecting and laser cut-off applications [53].

The direct and indirect band gaps have been computed from the absorption-edge using Tauc's formula and the absorption spectra [32],

$$\alpha h\upsilon = y(h\upsilon - E_g)^c \tag{5}$$

where α is the absorption coefficient, λ is the incident light wavelength, y is a constant, and c is a constant with allowed quantities of (1/2 and 2), not allowed quantities of (3/2 and 3) for direct and indirect transitions, respectively [39]. The values of direct and indirect bandgap are determined by the Tauc-plot curve of $(\alpha h\upsilon)^2$ and $(\alpha h\upsilon)^{0.5}$ versus $(\alpha h\upsilon)$ as it is shown in figure 9. Based on the Tauc-plot calculation, the direct and indirect bandgap values of the samples were estimated from the intercept of the energy axis. Table 1 summarizes the direct and indirect bandgap values. The bandgap decreases from 5.5 eV to 4.3 eV and from 4.9 to 2.5 eV for direct and indirect transition, respectively. The addition of Mn_2O_3/rGO NP in which Mn^{+3} ions exist in the matrix effects on the forbidden gap and produces defects between the valance and conduction bands [11]. These defects caused the formation of the localized states which increase by the increase in the defects in the matrix [11, 32]. The obtained results for this system are better than that for system of PVA-1.8 wt.% Mn_2O_3 [32] where the

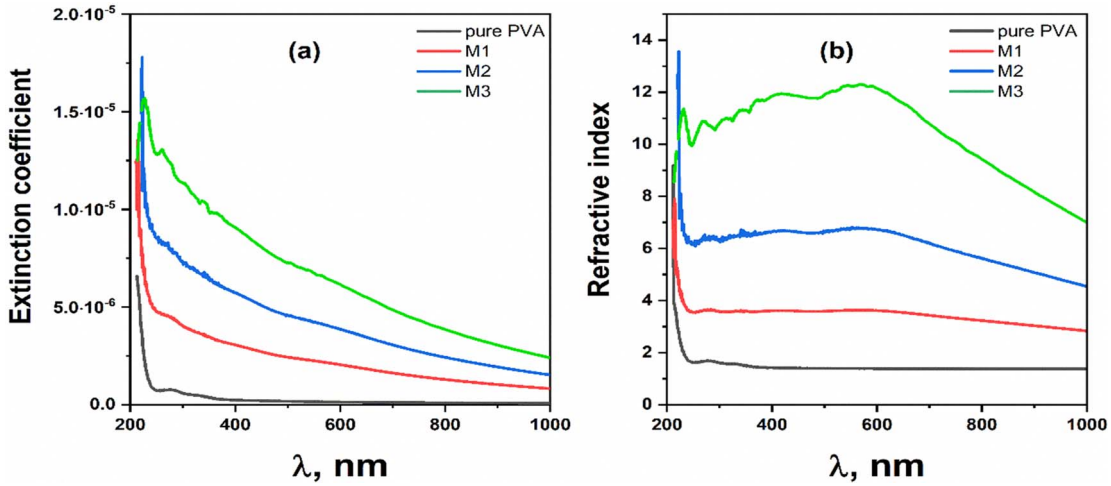

Figure 10. Plots of (a) extinction coefficient and (b) refractive index of PVA-Mn_2O_3/rGO composite films versus the wavelength.

bandgap decreased from 5.39 to 5.26 eV and from 5.03 to 4.63 eV for direct and indirect, respectively. This can be caused by the presence of rGO which increases the free ion number with higher mobility [27]. This effect increases with the increase in the Mn_2O_3/rGO concentration in the matrix.

3.4. Refractive index and extinction coefficient

The extinction coefficient (k), one of most significant optical characteristics, is described by the following formula [11];

$$k = \frac{\alpha\lambda}{4\pi} \tag{6}$$

Figure 10(a) shows the dependence of the extinction coefficient (k) on the wavelength for the polymer matrix with different Mn_2O_3/rGO NP concentrations. The extinction coefficient indicates the loss of light energy due to scattering and absorption [54]. It is clear that the higher value of k is in the UV-region. Its value decreases gradually as the wavelength increases. In addition, the k value increases with increasing the Mn_2O_3/rGO NP concentration in the PVA matrix. This is caused by the increase in the Mn^{+3} free ion numbers which absorb more energy [37].

The refractive index (n) was used to characterize the dispersion of electromagnetic waves of incident light into the material and it was obtained via the following equation [11];

$$n = \left(\frac{1+R}{1-R}\right) + \sqrt{\frac{4R}{(1-R)^2} - k^2} \tag{7}$$

wherein R indicates reflectance, [$R = 1-(T^* e^A)^{1/2}$], T is the transmission, and A is the absorption. Figure 10(b) shows the relationship between the incident wavelength and the refractive index (n) of the PVA-Mn_2O_3/rGO films. It is obvious that the refractive index increases as the Mn_2O_3/rGO NP concentration in the PVA matrix increases as well. This is caused by the increase in the density of free Mn^{+3} ions in the matrix [37]. These data are correlated with the absorption spectra (figure 8(a)).

3.5. Optical dielectric parameters and optical conductivity

Figure 11 shows the plots of dielectric constant (ε_r) and dielectric loss (ε_i) versus the wavelength of the incident light for PVA-Mn_2O_3/rGO composite films. The real component (ε_r) and imaginary component (ε_i) of the complex dielectric function are described by the following equations [5, 32]:

$$\varepsilon^* = \varepsilon_r + i\varepsilon_i \tag{8}$$

$$\varepsilon_r = n^2 - k^2 \tag{9}$$

$$\varepsilon_i = 2nk \tag{10}$$

where ε_r refers to the density of energy states and depends on electron mobility throughout light transformation in the medium and ε_i characterizes the absorbed energy due to the dipole motion [55].

The dielectric constant increases with the increase in Mn_2O_3/rGO NP in the PVA matrix. This is caused by the free Mn^{+3} ions which reduce the speed of light within the film [6]. Moreover, it can be related to the rise in the energy density of states of the PVA films with the increment of the NPs in the polymer matrix, which causes

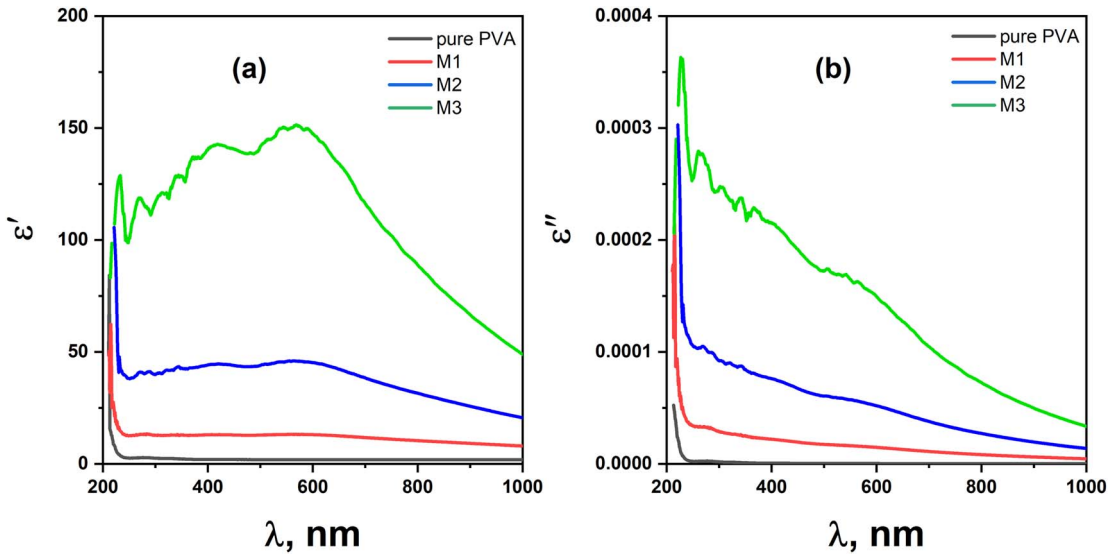

Figure 11. Plots of (a) ε' and (b) ε'' versus the wavelength of the incident light for PVA-Mn_2O_3/rGO composite films.

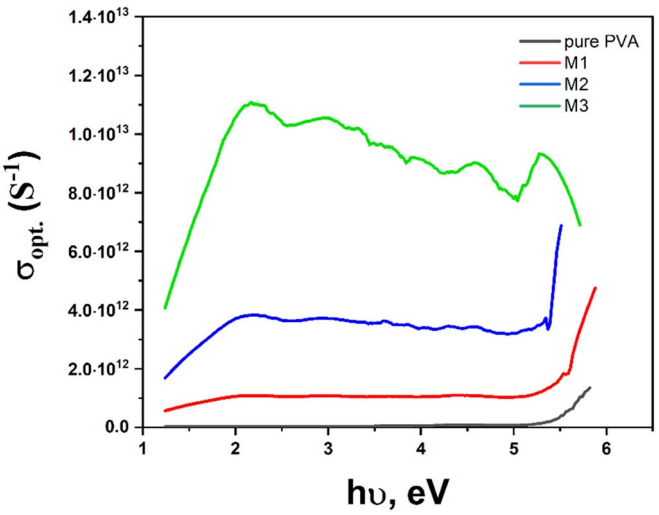

Figure 12. Plot of $\sigma_{opt.}$ versus $h\upsilon$ for PVA-Mn_2O_3/rGO composite films.

an increase in the polarization and ε' increases as well [9, 34]. The polymer films with high ε' value is highly appreciated in energy storage applications. While the dielectric loss is related to the absorption coefficient and to the dipole motions in the polymer matrix. Moreover, the dielectric loss characterizes the electronic transition from level to another. This behavior is correlated with the extinction coefficient.

Figure 12 shows the relation between the optical conductivity σ_{opt} and photon energy for the PVA films with different Mn_2O_3/rGO NP concentration. The optical conductivity $\sigma_{opt.}$ was calculated by the following equation [5, 56],

$$\sigma_{opt.} = \alpha n\, c/4\pi \tag{11}$$

where c is the speed of light. As the Mn_2O_3/rGO concentration increases, the optical conductivity increases as well. It may be caused by the increase in the Mn^{+3} free ion numbers [37]. In addition to the presence of the rGO sheets which raises polymer conductivity and ions mobility as well. As the photon energy increases in the range ($1.2 < h\upsilon < 2$ eV), the optical conductivity σ_{opt} increases as well, until it reaches its maximum value related to the Mn_2O_3/rGO concentration in PVA matrix. Whereas the optical conductivity is practically constant at $2.3 < h\upsilon < 5$ eV due to the normal dispersion of light. The optical conductivity rises exponentially in the vicinity of the absorption edge. This is due to an excess of free Mn^{+3} ion induced by incoming photon energy which is sufficient to overcome the band gap of the PVA-Mn_2O_3/rGO films.

4. Conclusion

The structure and optical properties of PVA-Mn_2O_3/rGO films are investigated. As the Mn_2O_3/rGO NP concentration increases in the PVA matrix the crystallinity degree decreases. It is caused by the hydrogen bonding between the Mn_2O_3/rGO NP and the hydroxyl group of PVA. As the Mn_2O_3/rGO NP concentration increases in the PVA matrix the cluster size increases as well. The surface roughness of the PVA-Mn_2O_3/rGO films increases with increasing the Mn_2O_3/rGO NP concentration confirming growth of the particle sizes in the matrix. The film transparency decreases with increasing the Mn_2O_3/rGO NP concentration due to increase in the Mn^{+3} free ion numbers which absorb more energy. The addition of Mn_2O_3/rGO NP in which Mn^{+3} ions exist into the matrix effects on the forbidden gap and produces defects between the valance and conduction bands Consequently, the optical band gap was found to decrease from 5.5 eV to 4.3 eV and from 4.9 to 2.5 eV for direct and indirect transition, respectively. Also, the refractive index and optical conductivity increase with increasing the Mn_2O_3/rGO NP concentration. The PVA-Mn_2O_3/rGO system with such optical properties is better than PVA-Mn_2O_3 system. In general, the produced films are more promising materials for various opto-electronic applications.

Data availability statement

All data that support the findings of this study are included within the article (and any supplementary files).

ORCID iDs

T S Soliman https://orcid.org/0000-0001-7372-4761

References

[1] Upadhyay R K, Soin N and Roy S S 2013 Role of graphene/metal oxide composites as photocatalysts, adsorbents and disinfectants in water treatment: a review *RSC Adv.* **4** 3823–51
[2] Nguyen T P 2011 Polymer-based nanocomposites for organic optoelectronic devices. A review *Surf. Coatings Technol.* **206** 742–52
[3] Soliman T S and Vshivkov S A 2019 Effect of Fe nanoparticles on the structure and optical properties of polyvinyl alcohol nanocomposite films *J. Non. Cryst. Solids.* **519** 119452
[4] Soliman T S, Vshivkov S A and Elkalashy S I 2020 Structural, linear and nonlinear optical properties of Ni nanoparticles—Polyvinyl alcohol nanocomposite films for optoelectronic applications *Opt. Mater. (Amst).* **107** 110037
[5] Ali H E, Morad I, Algarni H, El-Desoky M M, Khairy Y, Zahran H Y and Yahia I S 2021 Structure analysis and nonlinear/linear optical properties of PVAOH/Si composites for low-cost optical technologies and limiting absorption *J. Mater. Sci., Mater. Electron.* **32** 4466–79
[6] Aziz S B, Ahmed H M, Hussein A M, Fathulla A B, Wsw R M and Hussein R T 2015 Tuning the absorption of ultraviolet spectra and optical parameters of aluminum doped PVA based solid polymer composites *J. Mater. Sci., Mater. Electron.* **26** 8022–8
[7] Soliman T S, Vshivkov S A and Elkalashy S I 2020 Structural, thermal, and linear optical properties of SiO2 nanoparticles dispersed in polyvinyl alcohol nanocomposite films *Polym. Compos.* **41** 3340–50
[8] Soliman T S, Rashad A M, Ali I A, Khater S I and Elkalashy S I 2020 Investigation of Linear Optical Parameters and Dielectric Properties of Polyvinyl Alcohol/ZnO Nanocomposite Films *Phys. Status Solidi Appl. Mater. Sci.* **217** 2000321
[9] Abdullah O G, Aziz S B, Omer K M and Salih Y M 2015 Reducing the optical band gap of polyvinyl alcohol (PVA) based nanocomposite *J. Mater. Sci., Mater. Electron.* **26** 5303–9
[10] Issa S A, Zakaly H M H, Pyshkina M, Mostafa M Y A, Rashad M and Soliman T S 2021 Structure, optical, and radiation shielding properties of PVA–BaTiO3 nanocomposite films: An experimental investigation *Radiat. Phys. Chem.* **180** 109281
[11] Rashad M 2020 Tuning optical properties of polyvinyl alcohol doped with different metal oxide nanoparticles *Opt. Mater. (Amst).* **105** 109857
[12] Nawar A M, Mohammed M I and Yahia I S 2019 Facile synthesis and optical characterization of graphene oxide-doped TiO_2 /polyvinyl alcohol nanocomposites: optical limiting applications *Mater. Res. Express* **6** 075054
[13] Ali F M 2020 Synthesis and characterization of a novel erbium doped poly(vinyl alcohol) films for multifunctional optical materials *J. Inorg. Organomet. Polym. Mater.* **30** 2418–29
[14] Barandiaran I, Gutierrez J, Etxeberria H, Tercjak A and Kortaberria G 2019 Tuning photoresponsive and dielectric properties of PVA/CdSe films by capping agent change *Compos. Part A Appl. Sci. Manuf.* **118** 194–201
[15] Aziz S B, Hassan A Q, Mohammed S J, Karim W O, Kadir M F Z, Tajuddin H A and Chan N N M Y 2019 Structural and optical characteristics of PVA:C-dot composites: tuning the absorption of ultra violet (UV) region *Nanomaterials.* **9** 216
[16] Chebil A, Ben Doudou B, Dridi C and Dammak M 2019 Synthesis characterization, optical and electrical properties of polyvinyl alcohol/multi-walled carbon nanotube nanocomposites: a composition dependence study *Mater. Sci. Eng. B* **243** 125–30
[17] Abdel Salam M 2015 Synthesis and characterization of novel manganese oxide nanocorals and their application for the removal of methylene blue from aqueous solution *Chem. Eng. J.* **270** 50–7
[18] Nassar M Y, Amin A S, Ahmed I S and Abdallah S 2016 Sphere-like Mn_2O_3 nanoparticles: facile hydrothermal synthesis and adsorption properties *J. Taiwan Inst. Chem. Eng.* **64** 79–88
[19] Son Y H, Bui P T M, Lee H R, Akhtar M S, Shah D K and Yang O B 2019 A rapid synthesis of mesoporous Mn_2O_3 nanoparticles for supercapacitor applications *THE Coatings.* **9**
[20] Dakhel A A 2006 Correlated structural and electrical properties of thin manganese oxide films *Thin Solid Films* **496** 353–9

[21] Vignesh R, Prabha C N, Sivakumar R and Sanjeeviraja C 2022 Optical constants, optical dispersion and group index parameters of Mn_2O_3 thin films *Phys. B Condens. Matter.* **624** 413431
[22] Abdel-Salam A I, Awad M M, Soliman T S and Khalid A 2022 The effect of graphene on structure and optical properties of CdSe nanoparticles for optoelectronic application *J. Alloys Compd.* **898** 162946
[23] Li P, Zhu B, Li P, Zhang Z, Li L and Gu Y 2019 A facile method to synthesize CdSe-reduced graphene oxide composite with good dispersion and high nonlinear optical properties *Nanomaterials.* **9** 957
[24] Li Y, Lv X, Lu J and Li J 2010 Preparation of SnO_2-nanocrystal/graphene -*nanosheets composites and their lithium storage ability, J. Phys. Chem. C.* **114** 21770–4
[25] Geerthana M, Prabhu S, Harish S, Navaneethan M, Ramesh R and Selvaraj M 2022 Design and preparation of ternary α-Fe_2O_3/SnO_2/rGO nanocomposite as an electrode material for supercapacitor *J. Mater. Sci., Mater. Electron.* **33** 8327–43
[26] Abdel-Aal S K, Ionov A, Mozhchil R N and Naqvi A H 2018 Simple synthesis of graphene nanocomposites MgO–rGO and Fe_2O_3–rGO for multifunctional applications *Appl. Phys. A Mater. Sci. Process.* **124** 1–10
[27] Abdel-Salam A I, Attia S Y, El-Hosiny F I, Sadek M A, Mohamed S G and Rashad M M 2022 Facile one-step hydrothermal method for $NiCo_2S_4$/rGO nanocomposite synthesis for efficient hybrid supercapacitor electrodes *Mater. Chem. Phys.* **277** 125554
[28] Sharma S, Chauhan P and Husain S 2016 Structural and optical properties of Mn_2O_3 nanoparticles & its gas sensing applications *Adv. Mater. Proc.* **1** 220–5
[29] Gnanam S and Rajendran V 2013 Facile hydrothermal synthesis of alpha manganese sesquioxide (α-Mn2O3) nanodumb-bells: Structural, magnetic, optical and photocatalytic properties *J. Alloys Compd.* **550** 463–70
[30] Javed Q, Wang F P, Rafique M Y, Toufiq A M, Li Q S, Mahmood H and Khan W 2012 Diameter-controlled synthesis of α-Mn_2O_3 nanorods and nanowires with enhanced surface morphology and optical properties *Nanotechnology* **23** 415603
[31] Kalaiselvi C and Chandar N K 2021 Graphene decorated long single crystalline Mn2O3 nanorods: facile synthesis and visible light photocatalyst *Diam. Relat. Mater.* **120** 108703
[32] Khairy Y, Yahia I S and Elhosiny Ali H 2020 Facile synthesis, structure analysis and optical performance of manganese oxide-doped PVA nanocomposite for optoelectronic and optical cut-off laser devices *J. Mater. Sci., Mater. Electron.* **31** 8072–85
[33] Aslam M, Kalyar M A and Raza Z A 2017 Graphene oxides nanosheets mediation of poly(vinyl alcohol) films in tuning their structural and opto-mechanical attributes *J. Mater. Sci., Mater. Electron.* **28** 13401–13
[34] Badawi A and Alharthi S S 2022 The optical, electrical and mechanical performance of metal oxides incorporated PVA/rGO blend: effect of metal oxide type *Appl. Phys. A Mater. Sci. Process.* **128** 1–15
[35] Li Z, Ji X, Han J, Hu Y and Guo R 2016 $NiCo_2S_4$ nanoparticles anchored on reduced graphene oxide sheets: In-situ synthesis and enhanced capacitive performance *J. Colloid Interface Sci.* **477** 46–53
[36] Periyasamy G, Patil I M, Kakade B, Veluswamy P, Archana J, Ikeda H and Annamalai K 2022 Reduced graphene oxide-wrapped α-Mn_2O_3/α-MnO_2 nanowires for electrocatalytic oxygen reduction in alkaline medium *J. Mater. Sci., Mater. Electron.* **33** 8644–54
[37] Ali H E, Abdel-Aziz M M, Khairy Y, Zahran H Y, Algarni H, Yahia I S, El-Shamy E F, Sayed M A, Maged F A and Sanaa M F 2021 Microstructure analysis and nonlinear/linear optical parameters of polymeric composite films based PVAL for wide optical applications *Phys. Scr.* **96** 115804
[38] Morad I, Alshehri A M, Mansour A F, Wasfy M H and El-Desoky M M 2020 Facile synthesis and comparative study for the optical performance of different TiO2 phases doped PVA nanocomposite films *Phys. B Condens. Matter.* **597** 412415
[39] Ali F M and Maiz F 2018 Structural, optical and AFM characterization of PVA:La3 + polymer films *Phys. B Condens. Matter.* **530** 19–23
[40] Ali F M and Kershi R M 2020 Synthesis and characterization of La3 + ions incorporated (PVA/PVP) polymer composite films for optoelectronics devices *J. Mater. Sci., Mater. Electron.* **31** 2557–66
[41] Soliman T S, Hessien M M and Elkalashy S I 2022 Structural, thermal, and optical properties of polyvinyl alcohol films doped with La2ZnOx nanoparticles *J. Non. Cryst. Solids.* **580** 121405
[42] Rudawska A 2019 *Surface Treatment in Bonding Technology* (Academic Press: Elsevier) (https://doi.org/10.1016/B978-0-12-817010-6.09993-8)
[43] Gadelmawla E S, Koura M M, Maksoud T M A, Elewa I M and Soliman H H 2002 Roughness parameters *J. Mater. Process. Technol.* **123** 133–45
[44] Ali H E and Khairy Y 2020 Facile synthesis, structure, AFM, thermal, and optical analysis of BiI3/PVAL nanocomposite films for laser CUT-OFF optical devices *Vacuum* **180** 109640
[45] Marghalani H Y 2010 Effect of filler particles on surface roughness of experimental composite series *J. Appl. Oral Sci.* **18** 59–67
[46] Ullah R, Khan S A, Aladresi A A M, Alharbi S A and Chinnathambi A 2020 Ovalbumin-mediated synthesis and simultaneous functionalization of graphene with increased protein stability *Green Chem. Lett. Rev.* **13** 60–7
[47] Awad M M, Abdel-Salam A I, Elfeky S A, Rady H S, Hassanien A S, Mohamed M B and Elbashar Y H 2019 Tuning the optical properties of CdSe quantum dot using graphene nanocomposite *J. Opt.* **48** 616–25
[48] Khlyustova A, Sirotkin N, Kraev A, Agafonov A and Titov V 2021 Effect of metal oxides added onto polyvinyl alcohol via pulsed underwater plasma on their thermal, electrical and dielectric properties *J. Appl. Polym. Sci.* **138** 51174
[49] Abdel-Aziz M M, Algarni H, Elhosiny Ali H, Yahia I S, Khairy Y, Zahran H Y, Abdellahi M O, Al-Hagan O and Solyman S 2021 A novel polymer/ceramic composite film for different optical applications: Optical linear, nonlinear, and limiting properties *Phys. Scr.* **96** 055804
[50] Ali F M 2019 Structural and optical characterization of [(PVA:PVP)-Cu2+] composite films for promising semiconducting polymer devices *J. Mol. Struct.* **1189** 352–9
[51] Venkatachalam S 2016 Ultraviolet and visible spectroscopy studies of nanofillers and their polymer nanocomposites *Spectrosc. Polym. Nanocomposites* (British Library, William Andrew publications: Elsevier Inc) 130–57
[52] Aziz S B, Brza M A, Nofal M M, Abdulwahid R T, Hussen S A, Hussein A M and Karim W O 2020 A comprehensive review on optical properties of polymer electrolytes and composites *Materials (Basel).* **13** 3675
[53] Ali H E, Abdel-Aziz M M, Khairy Y, Zahran H Y, Algarni H, Yahia I S, El-Shamy E F, Sayed M A, Maged F A and Sanaa M F 2021 Microstructure analysis and nonlinear/linear optical parameters of polymeric composite films based PVAL for wide optical applications *Phys. Scr.* **96** 115804
[54] Mohamed M B and Abdel-Kader M H 2020 Effect of annealed ZnS nanoparticles on the structural and optical properties of PVA polymer nanocomposite *Mater. Chem. Phys.* **241** 122285
[55] Ismail M S, Elamin A A, Abdel-Wahab F, Elbashar Y H and Mahasen M M 2022 Improving the refractive index by engineering PbS/PVA nano polymer composite for optoelectronic applications *Opt. Mater. (Amst).* **131** 112639
[56] Choudhary S and Sengwa R J 2019 Investigation on structural and dielectric properties of silica nanoparticles incorporated poly (ethylene oxide)/poly(vinyl pyrrolidone) blend matrix based nanocomposites *J. Inorg. Organomet. Polym. Mater.* **29** 592–607